4.1 Introduction

The study of geometrically frustrated pyrochlore materials has received much attention due to its variety of low temperature ground states which is associated to the geometry of the spin lattice leading to frustration among the local spin interactions [1-3]. As a consequence of frustration, the spins cannot attain a long range order at low temperature but freeze in a random manner or remain dynamic down to lowest possible temperatures giving rise to exotic ground states. These special low temperature states include spin liquid states [4-9], apparent spin glass like states [10-15], spin ice state [16-21] and a state known as order by disorder [22-23] etc. These intriguing states are decided by balancing the strong crystal field effect (CFE), dipolar interactions and exchange interactions. The basic structure of pyrochlore $A_2B_2O_7$ is a derivative of fluorite type (CaF_2) structure which has two cations but one eighth fewer anions (i.e. an unoccupied interstitial site 8a surrounded by four B^{4+} cations) [24-25]. However, the pyrochlore structure is highly ordered as compared to fluorite where site disorder is present. An important parameter which decides the ordering of such $A_2B_2O_7$ structure is the co-ordination number. For, pyrochlore type structure, A (16d) and B (16c) ions are surrounded by 8 and 6 oxygen ions respectively while for fluorite type structure, B ions are prone to be in similar chemical surrounding like A ions (i.e. 8 O^{2-} ions). As the ionic radii of A and B cations come closer, the structure gradually transforms into anion disordered fluorite structure by the migration of some oxygen ions from 48f (O1) and/or 8b(O2) sites to the vacant 8a sites. In the unit cell of pyrochlore $Eu_2Ti_2O_7$, each Eu^{3+} (16d) is surrounded by eight oxygen atoms, thus forming a trigonally distorted cube in which six O-atoms situated at 48f sites are lying on the equatorial plane of the cube while the rest two O-atoms (8b) are lying diametrically opposite to each other along the <111> (D_{3D}) axis. On the other hand, the Ti^{4+} ions (16c) are lying adjacent to the vacant anion sites 8a and forming a distorted octahedron by the oxygen ions situated at 48f sites [24-25]. Obviously, the magnetic properties of these materials are mainly manifested by the electronic configurations of the *f* -rare earth ions R^{3+}. Due to strong CFE, the ionic magnetic susceptibility of R^{3+} ions differ along the D_{3D} axis and along the axis perpendicular to it, which eventually raises the single ion anisotropy (SIA)[26]. In spin ice materials which follow “ice rules”, the rare earth spins are highly uniaxial along <111> direction due to strong crystal field (CF) splitting driven SIA. As a consequence, a highly degenerate macroscopic ground state is observed at very low temperature (<4 K) for all spin ice materials. This happens because any state that follows “two in/two out” ice rule for all the tetrahedra is a ground state which leads to a huge number of degenerate low energy states [20-21,27-28]. Under this condition, the system cannot reach an ordered state by minimizing the dipolar interactions alone and hence ends up in a non-collinear, disordered and frozen state at very low temperature $T<T_{ice}$ ~4 K. Interestingly, of all the spin ice materials $Ho_2Ti_2O_7$, $Dy_2Ti_2O_7$, $Ho_2Sn_2O_7$, $Dy_2Sn_2O_7$ etc.; only $Dy_2Ti_2O_7$ shows a higher temperature spin freezing at 16 K along with its low temperature spin ice freezing at 4 K. This special higher temperature (~16 K) spin freezing for $Dy_2Ti_2O_7$ makes it more interesting towards various research communities and invited intense research attention towards this particular pyrochlore $Dy_2Ti_2O_7$. This 16 K spin freezing is attributed to single ion freezing and it is inter-linked with the low temperature ice freezing (<4 K) by a quantum tunnelling crossover process through the CF barrier and this is explained by creation and propagation of monopoles [29,30].

However, in the previous chapter, we have discussed about the observation of a new prominent spin freezing at around T_f ~35 K for $Eu_2Ti_2O_7$ (ETO), a temperature which is highest reported so far for such spin freezing due to geometrical spin frustration [31]. It has been inferred that the observed spin freezing is purely caused by local geometrical spin frustration where the spins have crystal field driven SIA which offers them less freedom for movement. The observed spin freezing is attributed to single spin relaxation process rather than a conventional spin glass freezing.

In various compounds having magnetic rare earth and transition metal ions in their composition are seen to exhibit several exotic phenomena including multiple magnetic transitions, spin reorientation transition; magneto-electric effect, magnetic field induced meta-magnetic transition etc owing to the existence of the different competing *f-f*, *f-d* and *d-d* exchange interactions [32-35]. In this context, we have incorporated Fe in ETO in the present work which is expected to add potential for producing interesting phenomena (since the configuration of 4*f* orbital is highly localized and much more complex than that of 3*d* orbital). DC magnetization measurements showed rise of ferromagnetic contributions below 100 K. In ac susceptibility, the spin freezing around 35 K is seen to get largely suppressed with Fe substitution. Most interestingly, an additional clear peak is observed in ac susceptibility ($\chi^{//}$) study in presence of magnetic field at lower temperatures (4 K<T^*<8 K). The observed new $\chi^{//}$ peaks are purely field induced and associated to Fe doping. The spin relaxation responsible for the observed peaks is unusually slow. We have emphasized on investigating the field induced ac $\chi^{//}$ peaks by varying both the fields and compositions to probe the possible origin of the peaks.

Moreover, a prior knowledge to the electronic states of the constituent ions essentially helps towards the understanding of origin of the structural and magnetic properties. Again, to date, the study of electronic structure of this system is hitherto unreported; hence we have investigated its XAS spectra also.

4.2 Experimental

4.2.1 Sample preparation

Polycrystalline $Eu_{2-x}Fe_xTi_2O_7$ (EFTO) (with x=0.0, x=0.1 and 0.2) samples were prepared by solid state reaction route. The flow chart of its preparation steps is shown in below:

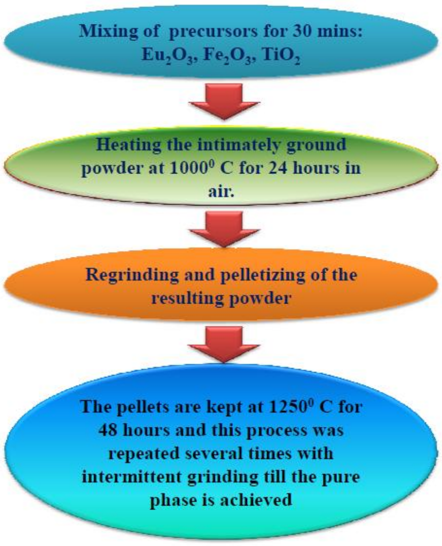

Figure. 4.1: *The flow chart for the sample preparation.*

High purity (>99.99%) Eu_2O_3, Fe_2O_3 and TiO_2 were mixed in stoichiometric ratio and ground for 0.5 hr, then heated in air at 1000^0 C for 24 hours. The resulting powder was reground and pressed into pellets and heated in air at 1250^0 C for 48 hours and the process was repeated several times.

4.2.2 Characterization techniques

Analysis of X-ray powder diffraction (XRD) measurements confirm the prepared samples are of single phase with no chemical phase impurity. All the magnetic measurements were performed using a Quantum Design magnetic property measurement system (MPMS) super conducting quantum interference devices (SQUID) magnetometer. The XAS measurements at FeL_{2-3} and EuM_{4-5} edges were carried out at the BL-14 beamline of Hiroshima Synchrotron Radiation Center (HiSOR), Hiroshima University, Japan. The XAS measurements at TiL_{2-3} and O K edges were performed at

Raja Ramanna Centre for Advanced Technology (RRCAT), Indore in INDUS 2 BL-1 beamline. In our case, total electron yield (TEY) mode has been used because of its high surface sensitivity with high signal to noise ratio.

4.3 Results and Discussions

4.3.1 Structural study

We have examined the crystalline structure of the samples by refining the XRD data by Rietveld method using Fullprof software. The XRD pattern of all the three EFTO (x=0, 0.1, 0.2) samples along with its refinement is shown in Fig. 4.2. It suggests that the samples crystallize in pure cubic phase (space group *Fd-3m*) without any traces of impurities and the detailed crystallographic information have been summarized in the Table 4.1. A pictorial representation of the crystal structure obtained through its refinement is shown in the upper inset of Fig. 4.2. The refinement shows linear decrease in lattice constants (a=b=c) with increasing Fe concentration which accords the Vegard's law (since ionic radius of Fe^{3+} is smaller) [36], thus suggesting a homogenous solid solution of Eu/Fe mixture [inset (bottom) of Fig.4.2]. As a result of Fe doping, the effective cell volume of the lattice as well as the effective Eu-Eu, Eu-O, Eu-Ti bond lengths decrease systematically and eventually modifies the exchange interactions which is manifested in their magnetic behaviours. Moreover, the octahedral distortion is evident from the obtained bond angles measured on the equatorial plane of the octahedron. The estimated bond angles of O1-Ti-O1 are found to be 94.514^0 and 85.486^0 (which are observed to remain almost unchanged with Fe doping : Table-4.1) which are close to the bond angle values ~92.5^0 and ~87.5^0 reported for a similar pyrochlore with TiO_6 octahedral distortion [37].

Table 4.1: Structural parameters and crystallographic sites determined from Rietveld profile refinement of the powder XRD patterns for pyrochlore $Eu_{2-x}Fe_xTi_2O_7$ at 300 K (room temperature).

Space group: F d $\bar{3}$ m

Parameters	X=0	X=0.1	X=0.2
Lattice constant (Å)	a=b=c= 10.18645(8)	a=b=c= 10.1722	a=b=c=10.1570
Cell volume (Å^3)	1056.9840	1052.5547	1047.8527
Eu site	16d	16d	16d
x	0.5	0.5	0.5
y	0.5	0.5	0.5
z	0.5	0.5	0.5
Fe site	16d	16d	16d
x	0.5	0.5	0.5
y	0.5	0.5	0.5
z	0.5	0.5	0.5
Ti site	16c	16c	16c
x	0.0	0.0	0.0
y	0.0	0.0	0.0
z	0.0	0.0	0.0
O(1) site	48f	48f	48f
x	0.31870	0.32495	0.32902
y	0.125	0.125	0.125
z	0.125	0.125	0.125
O(2) site	8b	8b	8b
x	0.375	0.375	0.375
y	0.375	0.375	0.375
z	0.375	0.375	0.375
R_{wp}	29.8	25.4	25.4
R_{exp}	17.01	16.06	15.75
R_{wp}/R_{exp}	1.75	1.51	1.61
Chi^2	3.06	2.49	2.37
d_{Eu-Eu}(Å)	3.601454	3.59642(10)	3.59105
$d_{Eu-O(1)}$(Å)	2.512442(12)	2.50893(6)	2.50519
$d_{Eu-O(2)}$ (Å)	2.205431(10)	2.20235(5)	2.19906
$d_{Ti-O(1)}$ (Å)	3.79552(2)	3.79021(12)	3.78455
$d_{O(1)-O(2)}$ (Å)	3.02537(2)	3.62805(10)	3.62264
$d_{Fe-O(1)}$ (Å)	-	4.65409(16)	4.64715
<(Eu)-(O1)-(Eu)>(deg)	139.8122 (13)	139.812(6)	139.81218
<(Eu)-(O2)-(Eu)>(deg)	109.4712(9) -	109.471(5)	109.47123
<(Eu)-(O1)-(Fe)>(deg)	-	139.812(6)	139.81218
<(Ti)-(O1)-(Fe)>(deg)	-	106.350(5)	106.35051
<(Fe)-(O1)-(Fe)> (deg)	-	139.812(6)	139.81218
<(Ti)-(O1)-(Ti)> (deg)	132.9695(15)	132.382(6)	132.3825
<(O1)-(Ti)-(O1)>	94.5139 (8)	94.514 (4)	94.51386
<(O1)-(Ti)-(O1)>	85.4861(11)	85.486 (6)	85.48614

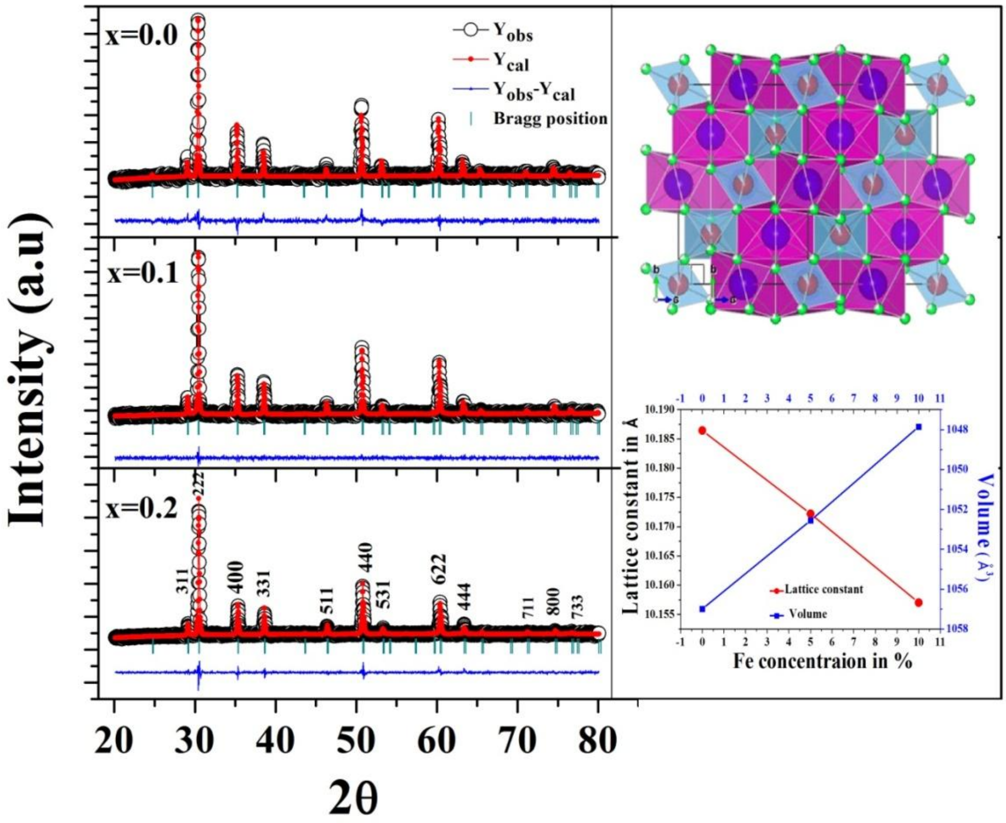

Figure 4.2: *Rietveld refinement of X-ray diffraction pattern collected at room temperature (300K) of EFTO. The black and red lines stand for experimental and fitted intensities respectively. The difference is shown at the bottom. The vertical bars representing the allowed reflections. Inset (top) : Polyhedral pictorial representation of the crystal structure, here the blue, red and green spheres are representing* Eu^{3+}, Ti^{4+} *and* O^{2-} *ions. Inset (bottom): lattice parameter and cell volume variation as a function of doping concentration.*

4.3.2 X-ray absorption spectroscopy (XAS) study

In order to probe the electronic structure and get insight into the local structural order of the present systems, XAS spectra have been recorded at room temperature. Figure 4.3(a) shows Fe 2*p* XAS spectrum corresponding to the photo-absorption from Fe2*p* core level to the Fe 3*d* or 4s unoccupied states for x=0.1 sample (ETOF5). It consists of two peaks

FeL_3($2p_{3/2}$) and FeL_2($2p_{1/2}$) at ~ 710 eV and~ 724 eV, respectively, which is separated due to the spin-orbit interaction (ΔE~14 eV). Notably a small but distinct crystal field splitting in the t_{2g} peaks of both FeL_3 and FeL_2 are discernible which indicates localized nature of Fe 3*d* electrons. The spectral features are essentially similar to the Fe2*p* XAS spectra of the well-studied γ-Fe_2O_3 system, where the Fe ions lie in tetrahedral and octahedral coordination with oxygen ions [38]. The shape of the XAS spectra is significantly different from that of α-Fe_2O_3 where the splitting of Fe2p$3_{/2}$ is more pronounced due to the crystal field splitting as Fe^{3+} ions occupy only the octahedral (O_h) sites [38]. Thus, it confirms the nominal valency of 3+ for Fe ions in the present system and also the successful substitution of Eu ions by Fe ions [38]. The Fe2*p* XAS spectral feature excludes contributions from the Fe^{2+} spectral features as typically seen in metallic Fe, FeO or Fe_3O_4, suggesting absence of any mixed-valence states. Fig. 4.3(b) shows the Eu3*d* XAS spectrum at Eu$M_{4,5}$ edges at 300 K for ETOF5, which corresponds to the dipole transition from Eu3*d* core level to unoccupied Eu4*f* state. Two prominent peaks are observed corresponding to the EuM_5 ($3d_{5/2}\rightarrow 4f$) at ~1131.2 eV and EuM_4 ($3d_{3/2}\rightarrow 4f$) at ~1158.9 eV, which are separated by the spin-orbit interaction (energy ΔE ~27.7 eV). The Eu3*d* XAS spectra is similar to that of Eu_2O_3 [39], but different from that of EuO. The 3+ oxidation state of Eu ions (for ETOF5) can be evident from two clearly visible shoulder peaks A and B at ~1125.7 eV and ~1135.1 eV which are the signatures of 3+ oxidation states. Note that while Eu^{3+} is non-magnetic in its $^7F_0$ ground state, its subsequent excited states $^7F_{1,2,3}$ are magnetic [26,39], leading to appreciable magnetic moment for this ion.

Fig. 4.3(c) depicts the room temperature Ti2*p* XAS spectra at Ti$L_{2,3}$ edges for all three samples (ETO [x=0.0], ETOF5 [x=0.1] and ETOF10 [x=0.2]). The Ti2*p* XAS spectrum is associated to the transition of electrons from Ti2*p* to Ti3*d* states. By comparing the line shape and energy separation between the obtained peaks with previously reported Ti2*p* XAS spectra for TiO_2, Ti_2O_3, $BaTiO_3$, $SrTiO_3$, the observed spectra are found to accord with those of TiO_2, $SrTiO_3$, $BaTiO_3$ suggesting nominal oxidation state is Ti^{4+} [38,40-43]. The four peak structure of the spectra includes the spectral features denoted as A, B corresponding to the Ti$L_3(2p_{3/2})$ absorption while C, D to the Ti$L_2(2p_{1/2})$ absorption. The single sharp nature of the peak A is indicating the octahedral co-ordination of the Ti^{4+} ions. The spin-orbit splitting energy is found to be ~5.35 eV for all the three samples. These spectral features are further split due to the crystal field, corresponding to the t_{2g} and e_g sub-bands. There is noticeable changes in the crystal field splitting energies (10 Dq) with the Fe doping as they are found to be ~ 2.4 eV, 2.2 eV and 2.1 eV for x=0.0, 0.1 and 0.2 respectively which suggest altered local environment of Ti. Moreover, TiL_3-e_g peak further splits into an asymmetric doublet denoted by **B** and **B**$^{/}$. Eventually, the e_g states (consisting of two orbitals $d_{x^2-y^2}$ and d_{z^2}) are highly sensitive to any distortion in TiO_6 octahedra. It is relevant to mention here that similar e_g splitting was observed in TiO_2 having octahedral distortion, unlike $SrTiO_3$ or $BaTiO_3$ in which Ti is in perfect O_h symmetry [38,40-43]. We reiterate that the octahedral distortion was also predicted by our XRD analysis. Hence, presence of a distorted O_h symmetry for the present system can be inferred. Moreover, it was seen that TiO_2 with rutile and anatase phases having tetragonal distortions show a clear asymmetric doublet whereas a single symmetric peak is observed for ilmenite phase having trigonal octahedral distortion [44-45]. Thus, our data clearly suggest towards tetragonal distortion of the TiO_6 octahedra. It can be noted that the e_g splitting is reduced with increased Fe doping (ΔE ~ 0.93 eV, 0.72 eV and 0.63 eV are found for samples x=0.0, 0.1 and 0.2 respectively). This suggests that octahedral distortion gradually diminishes by Fe substitution. Apart from this, the peak D shifts towards lower energy thus lowering the energy difference ΔE between C and D peaks with Fe substitution. Again, the intensity height ratio of these two peaks C and D (C peak is fitted with single peak with intensity I_C while D peak is fitted with two peaks with intensities I_{D1}

and I_{D2} due to its shoulder at higher energy i.e. the ratio is $I_C/I_{D1}+I_{D2}$) is found to diminish with Fe doping (not shown). Similar features were observed in a pyrochlore system $Nd_{2-x}Y_xZr_2O_7$ due to substitution of smaller cations Y^{3+} in the Nd^{3+} site [46].Where, due to transfer of 48*f*/8*b* oxygen ions to 8*a* sites; the local co-ordination of Zr ions changes from 6 to 7 leading to local anionic disorder [46]. Hence, it is plausible to explain that smaller Fe^{3+} ions (since, large difference between A and B ionic radii is a perquisite to ordered pyrochlore structure) substitution caused migration of 48f/8b oxygen ions to the 8*a* site, thus leading to the gradual increase in local anti-site anion disorder which in turn diminishes the O_h distortion in EFTO. However, the observation of relatively less L_3-e_g splitting for present systems as compared to that of TiO_2 (ΔE~0.93 eV) suggests for relatively a smaller distortion from the perfect O_h symmetry for EFTO [40].

However, this explanation of e_g splitting still remains under debate because the distortion effect is too weak to produce significant e_g splitting [47]. Later, P. Kruger claimed that the e_g splitting is not related to local structural effect rather is associated to long range structural effects [48]. He theoretically showed that experimentally observed L_3-e_g splitting could only be reproduced by taking at least an array of 60 atoms and hence this is a “non-local” effect having a length scale of 1 nm [48]. Thus, the observed diminishing e_g-splitting feature can be elucidated on the basis of the decreased long range structural order of the system by random Fe substitution in the A site as well as by increased anionic disorder.

Two weak satellite peaks marked as S1and S2 at photon energies ~473 eV and ~476.7 can also be observed (Fig. 4.3c). These peaks are associated to the hybridization of Ti 4*p*, Ti 3*d* and Ti 4*s* states with ligand orbitals O 2*p* which occurs due the charge transfer process [49-50].

Fig. 4.3(d) shows the XAS spectra recorded at O *K* edge for EFTO. It consist of two main regions:1) the region between the energy ~530 eV to 536 eV comprises of peaks A and

B (identified as t_{2g} and e_g states and arises due to hybridization of empty O*2p* orbitals to the Ti*3d*, Fe*3d* and Eu*4d* orbitals) which is sensitive to the ligand co-ordination and the local crystal symmetry. 2) Region above ~ 537 eV (resulting from the longer overlap of O*2p* orbitals to the Ti, Fe 4*sp* and Eu*5sp* orbital) which is associated to the long range structural ordering of the system [41,44].

It can be noted that the crystal field splitting ΔE between t_{2g} and e_g peaks decreases gradually with increasing Fe substitution. Here, the peak A remains merely fixed while the B peak shifts towards the lower energy (535.1 eV to 534.5 eV) which is consistent with the previous TiL_{2-3} edge spectra. Again, this effect can be attributed to the change in the local environment (increase in the co-ordination) around Ti^{4+} ions [46].

Moreover, looking at the second region (>537 eV), we can observe a prominent peak C which is followed by two broad features D and E which are originated from the hybridization of O*2p* and metallic *s-p* states [41]. Again gradual shift of peak C can presumably be ascribed to the additional contribution coming from Fe*4s-p* states to the existing Ti*4s-p* and Eu*5s-p* states. A noticeable change can be observed in the broad features D and E which are flattened and gradually become weak as Fe concentration is increased. This is a clear indication of increasing disorder in the system (as broadening of these spectral features is known to be related to the diminishing long range structural order) [51].

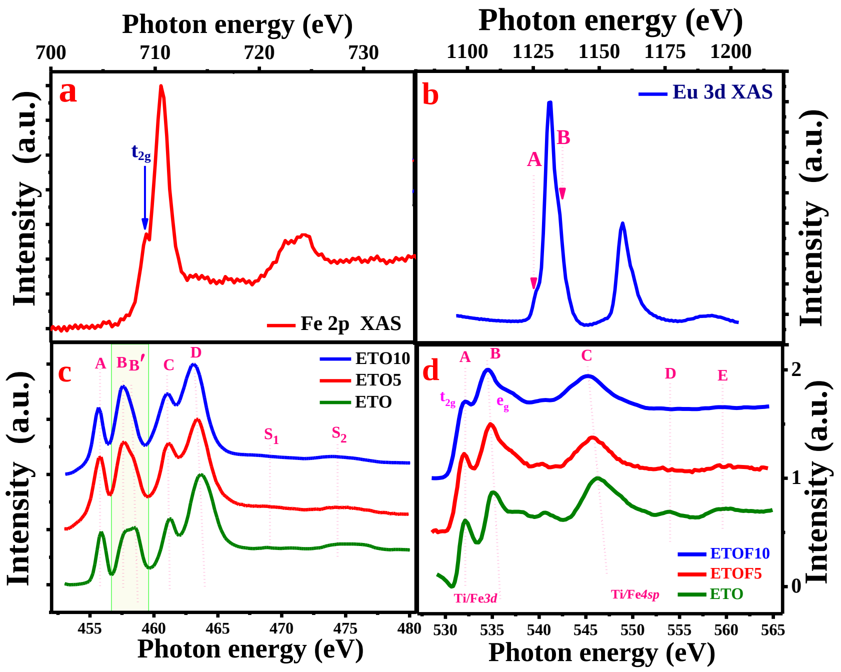

Figure. 4.3: *Fig. (a): Fe 2p XAS spectra at $L_{2,3}$ edges recorded at 300K. Fig(b) : Eu 3d XAS spectra at M4-5 edges at 300K. Fig. (c) and (d) are showing the $TiL_{2\text{-}3}$ and O K XAS spectra (for x=0.0, 0.1 and 0.2 samples) respectively.*

4.3.3 DC magnetization study

DC magnetization measurements were carried out as a function of temperature and magnetic field. Fig. 4.4 (a-c) shows the M (T) curves following the zero field (ZFC) and field cooling (FC) protocols with H=100 Oe for all the three samples. The magnetization (M) for pure sample (x=0.0) increases with decreasing temperature down to 90 K where it enters merely in a plateau region extending down to 20 K (Fig. 4.4a). This plateau region was attributed to the CFE [52]. For the whole temperature range (2-300 K), the M (T) curve does not follow the standard Curie-Weiss (CW) law: $\chi = \frac{M}{H} = \frac{C}{T-\theta_{CW}}$, here C is the Curie constant and θ_{CW} is the CW temperature. However, an attempt to fit the M-T curve with Curie-Weiss law below 100K was successful, suggesting the system remains paramagnetic down to lowest available temperature ~2 K (Inset of Fig. 4.4(a)). The small bifurcation or thermo-magnetic irreversibility observed between the ZFC and FC curves suggests existence of spin frustration in this system. This bifurcation was completely vanished while higher field was applied which confirmed it to be different from typical spin glass [31]. On the contrary, negligible bifurcation (as compared to pure sample) can be observed for the doped systems, thus suggesting that doping relieved the spin frustration (Fig. 4.4b and 4.4c and their sub-insets). However, the magnetization value is drastically enhanced with Fe^{3+} ion substitution which can be attributed to the exchange interactions between Eu-Fe and Fe-Fe spins and to the larger moment of Fe^{3+} spins (Fig. 4.4

(b-d)). It has also completely suppressed the plateau region. For the doped samples, M is observed to increase with decreasing temperature and no magnetic phase transition is observed which can be ascribed to the positive *f-d* super exchange mechanism [53]. As a matter of fact, in each tetrahedron of the pyrochlore system, there is on an average very few Fe^{3+} ions since the concentration of Fe^{3+} doping is very low (up to 10%). Thus, Fe^{3+} ions cannot form its nearest neighbour pair with another Fe^{3+} ion and consequently the direct exchange interaction between Fe-Fe is very weak. Hence, Eu-Fe spin interactions (*f-d*) play the main role in altering the magnetic behaviour of EFTO. Moreover, as evident from XRD analysis, the Fe substitution reduces the effective Eu-Eu distances which in turn enhance the exchange interactions among these spins. However, M (T) curves for both the doped samples were fitted well by CW law above ~ 100 K, this indicates that the system remains paramagnetic down to ~100K below which it deviate from CW behaviour (inset of Fig. 4.4 (b and c)). This directly suggests that it do not remain simply paramagnetic instead ferromagnetic contribution comes into play below 100 K. Factually, the sharp rise in magnetization below ~20 K is seemingly associated to some type of magnetic ordering. To confirm it, the curves were fitted with standard three dimensional (3D) spin wave model: M(T)=$M(0)(1-AT^{\frac{3}{2}})$, where M(0) is the saturation magnetization related to the ferromagnetic contribution at T=0 K and A being a parameter associated to the structural properties of the system [54]. However, the fitting was not satisfactory for both the Fe doped samples (not shown). However, a combination of these two models i.e. M(T)=$\frac{(C\times H)}{T-\theta_{CW}}+M(0)(1-AT^{\frac{3}{2}})$ was found to result in a reasonably good fitting as can be seen from the inset of Fig. 4.4(b-c). The first term of the above expression related to the paramagnetic contribution dominates at relatively higher temperatures (>20 K) whereas the second term pertaining to the ferromagnetic component dominates in the comparatively lower temperature region (<20 K) where sharp rise in magnetization occurs. Thus, it clearly suggests the existence of ferromagnetic contribution along with the paramagnetic phase at lower temperatures (<100 K). Further investigations have been done by recording M(T) curves with higher magnetic fields as shown in the inset 1 and 2 of Fig. 4.5 for x=0.1 and 0.2 samples respectively. The curves at lower temperature region can be seen to show very strong field dependence. Typically, such strong field dependence of the magnetization also suggests towards the existence of magnetic ordering in the lower temperature region.

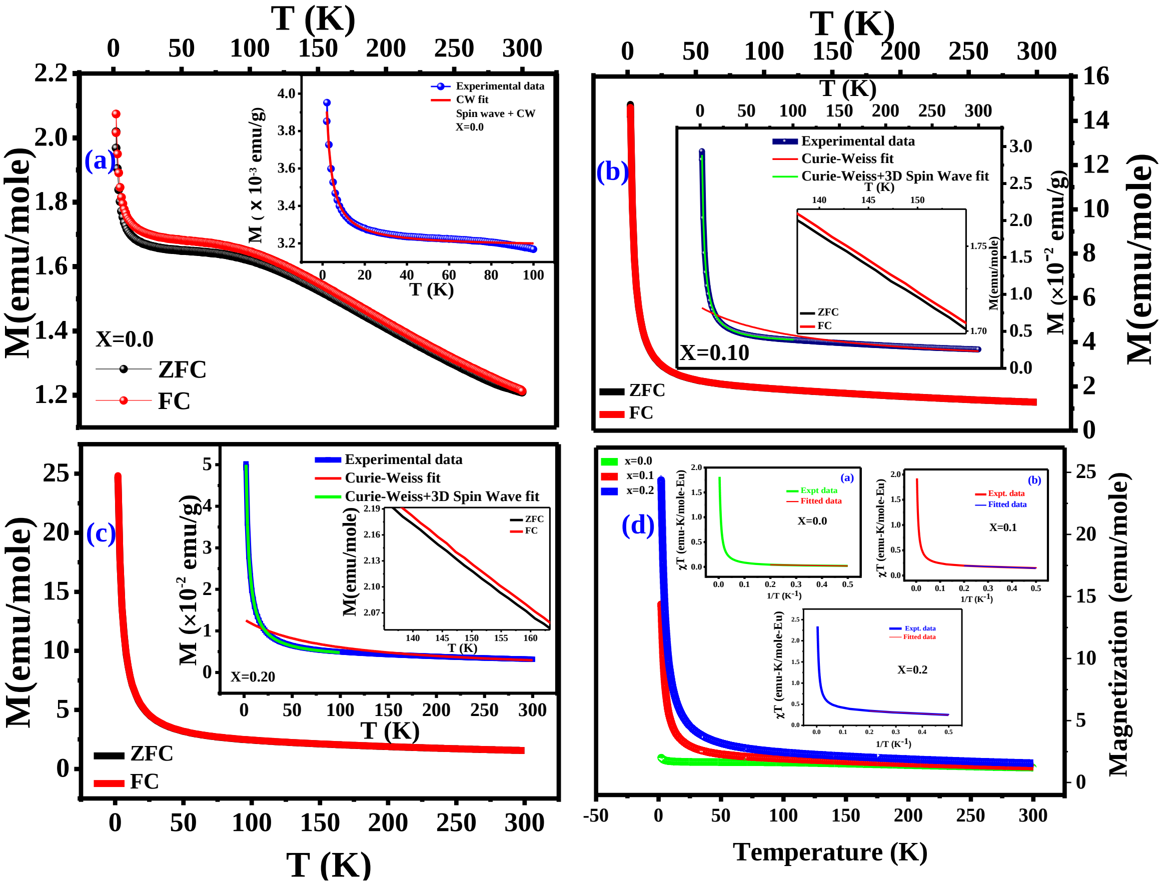

Figure. 4.4: *Fig. (a,b and c) shows the ZFC and FC M(T) curves recorded with applied field of H=100 Oe for the samples x=0.0, 0.1 and 0.2 respectively. Fig. (d) shows the comparison of dc M(T) curves(at 100 Oe) for the samples withx=0.0, 0.1 and 0.2. Inset of Fig. (a): Combined 3D spin-wave model andCW fit. Inset of Fig. (b) and (c) show the CW fit for the range 100-300 K and combined CW-3D spin wave model fit for 2-100 K for the Fe doped samples x=0.1 and 0.2 respectively. Inset figures (a), (b) and (c) of Fig. (d) showing"high temperature series expansionof susceptibility (χ) fitting" of curve "**χT Vs 1/T**" for x=0.0, 0.1 and 0.2 samples. Sub-inset of Fig. (b) and (c) are showing a closer view of the ZFC-FC curves for x=0.1 and 0.2 respectively.*

Understanding the fact that the sharp rise in magnetization cannot be attributed to CFE alone, other magnetic interactions, e.g., exchange interactions, dipolar interactions etc., should be taken into considerations. Therefore, high temperature series expansion of the susceptibility $(\chi) = \mathbf{C}\,[\frac{1}{T} + \frac{\theta_{cw}}{T^2}]$ is considered to estimate contributions of different exchange interactions [52,55]. From linear fit of the plot "χ**T** Vs $\frac{1}{T}$" for the temperature range 2-5 K, the values of Curie Weiss temperature Θ_{cw}, effective magnetic moment μ_{eff}, exchange interaction energy J_{nn} and dipolar interaction energy D_{nn} were calculated (inset a,b and c of Fig.4.4 (d)). Here, $J_{nn} = \frac{3\Theta_{cw}}{zS(S+1)}$, where z=6 be the co-ordination number. μ_{eff} was determined using the relation $C= \frac{N\mu_{eff}^2}{3K}$ and the D_{nn} was obtained from $D_{nn}= \frac{\mu_{eff}^2\mu_0}{4\pi r_{nn}^3}$ where r_{nn} refers to the distance between a Eu^{3+} ion at (000) and its nearest neighbour at (*a*/4,*a*/4,0), *a* being the lattice constant of the unit cell [52,56]. The calculated values are summarized in Table-4.2. The data obtained for pure (x=0.0) sample indicates that nearest neighbour AFM J_{nn} energy dominating over FM D_{nn} energy while Θ_{cw} is found to be slightly negative (-1.35 K). These results are in well agreement with the previous report [52]. It is evident from Table-4.2 that FM D_{nn} and μ_{eff} increase appreciably with Fe substitution. Interestingly, it can be noted that AFM J_{nn} energy initially decreases with Fe doping (x=0.1) but with further doping (x=0.2) it has increased slightly. Similar behaviour is observed for Θ_{cw} also. As a matter of fact, the Eu -Fe spin interactions seem to play an important role in manifesting such anomalous behaviour. Initially for x=0.1 sample, Θ_{cw} becomes less negative suggesting a rise in ferromagnetic interactions in the system. Here, the FM Eu-Fe interactions remain dominating over AFM Fe-Fe interactions (since Fe concentration is very low). However, as Fe concentration increases to x=0.2, the AFM Fe-Fe interactions slightly increase, thereby pushing the Θ_{cw} towards slightly more negative side.

Table-4.2: **Showing the magnetic characteristic parameters evaluated from high temperature series expansion of susceptibility study for the temperature range 2K-5K for all three samples (x=0, 0.1, 0.2).**

Sample $Eu_{2-x}Fe_xTi_2O_7$	Curie-Weiss temperature(Θ_{cw})	Effective magnetic moment (μ_{eff})	Exchange interaction energy (J_{nn})	Dipolar exchange interaction energy (D_{nn})
X=0.0	**-1.35K**	**0.679 μ_B**	**-0.67K**	**+0.006K**
X=0.1	**-0.72K**	**1.346 μ_B**	**-0.36K**	**+0.024K**
X=0.2	**-0.79K**	**1.801 μ_B**	**-0.39K**	**+0.045K**

Further investigations have been done by measuring the isothermal field dependent magnetization (M-H) at 2 K (Fig. 4.5). The unsaturated linear nature of the M-H curve for the pure sample suggests that the paramagnetic phase prevails even at a temperature ~2 K. However, the appearance of non-linearity in M(H) curves and rise in magnetization for doped samples (x=0.1, 0.2) indicate effective rise of ferromagnetic contribution. On the other hand, unsaturated nature of the magnetization upto 2 T, indicates strong antiferromagnetic interactions are also present in the system. A close observation reveals the coercivity of the hysteresis loop also increases with doping (inset 3 of Fig. 4.5). Thus, it agrees with our previous M(T) data.

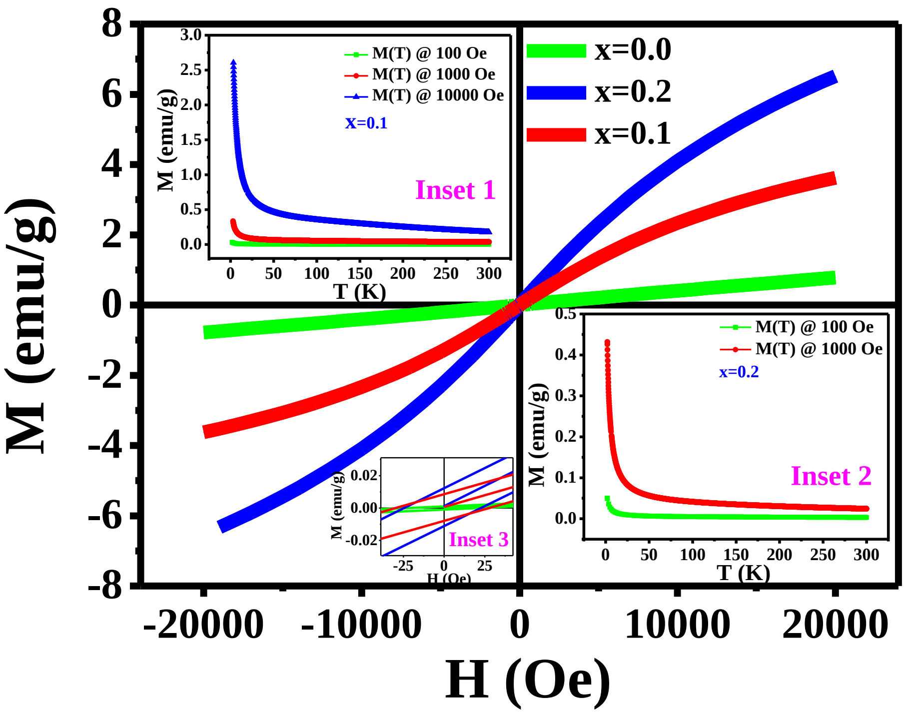

Figure. 4.5: *Isothermal magnetization curves as a function of magnetic fields at temperature 2K. Inset 3 showing a close view of the curve. The inset 1 and 2 are showing the M (T) curves at different applied fields.*

4.3.4 AC magnetization study

In contrast to dc magnetization study, ac-susceptibility study allows us to probe the spin dynamics in the system [57]. Hence, to examine how Fe substitutions alter the spin dynamics of the system, we have studied ac susceptibility of EFTO. For pure sample (ETO), we have already reported a spin freezing transition at a temperature ~35 K which is highest reported so far for such pyrochlore systems [inset of Fig. 4.6(c) and 4.6(d)][31]. The spin freezing was observed as a sudden drop in ac susceptibility $\chi^{/}$(in phase part), while its corresponding Kramers-Kronig frequency dependent peaks were found in ac $\chi^{//}$(quadrature part) below ~35 K. The peaks were observed to follow the Arrhenius law $f = f_0 e^{-E_b/K_B T}$, thus confirmed it to be a thermally activated process with an activation energy barrier E_b=339 K. The underlying physics behind such transition was elucidated by a single ion relaxation process of Eu^{3+} spins unlike the conventional spin glass process [58].

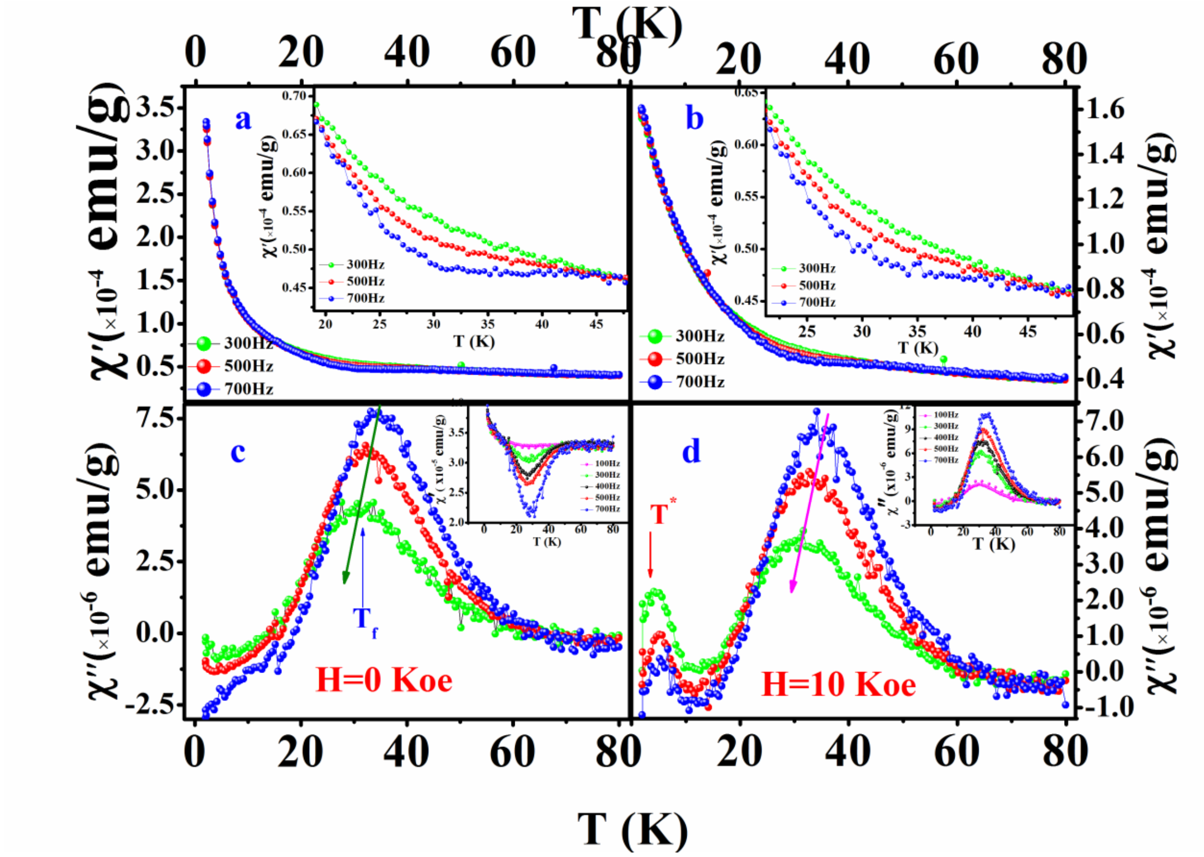

Figure. 4.6: *(a) and (c) showing temperature variation of* χ' *and* χ'' *@H=0 KOe while (b) and (d) showing* χ' *and* χ'' *@H=10KOe for x=0.1 sample. Inset of (a) and (b): Enlarged view of* χ' *(T) with H=0 KOe and 10Koe respectively, showing frequency dependence is still present in the system. Inset of (c) and (d): The temperature variation of* χ' *and* χ'' *at different frequencies for pure* $Eu_2Ti_2O_7$ *at H=0 KOe.*

Fig. 4.6 (a&c), show the temperature variation of ac χ' and χ'' of sample ETOF5 with H=0 Oe. The substitution of as little as 5% Fe, has caused a dramatic change in the nature of the χ' curves, as the frequency dependence of χ'curves have become very weak while its drop below the freezing temperatures (T_f ~ 35 K) is almost disappeared (Fig. 4.6a). The curve χ' shows a monotonous rise with increasing slope as temperature decreases for all the excitation frequencies, a feature which is completely different from that of sample ETO. This is in strong contrast to the magnetic behaviour observed in the non-magnetic diluted system where the spin freezing transition was observed to be enhanced [31]. Eventually, little substitution of Fe^{3+} ions causes local disorder (as evident from XAS analysis) that is sufficient to disrupt the crystalline field spacing of Eu^{3+} ions, which causes significant suppression of the spin freezing. The suppression of the spin freezing in $\chi^{/}$, clearly indicates a faster spin relaxation occurring in the system. A close observation reveals that weak frequency dependence is still present in the system (inset of Fig. 4.6(a)).

On the contrary, observation of clear peaks in $\chi^{//}$ confirms that spin relaxation is still present in the system (Fig. 4.6(c)). Arrhenius fit to the $\chi^{//}$ peaks yielded a value of E_b=316 K for ETOF5. So, the observed faster spin relaxation thus can be explained on the basis of decreased thermal energy barrier which offers the spins less time to relax. The decrease in the energy E_b is seemingly due to the little modification in the CF levels and change in the spin-phonon spectrum associated with small changes in lattice constant and electronic structure of the system [59]. Moreover, a close observation reveals a minute shift of the freezing temperature T_f towards lower temperature with Fe doping (inset of Fig. 4.7).

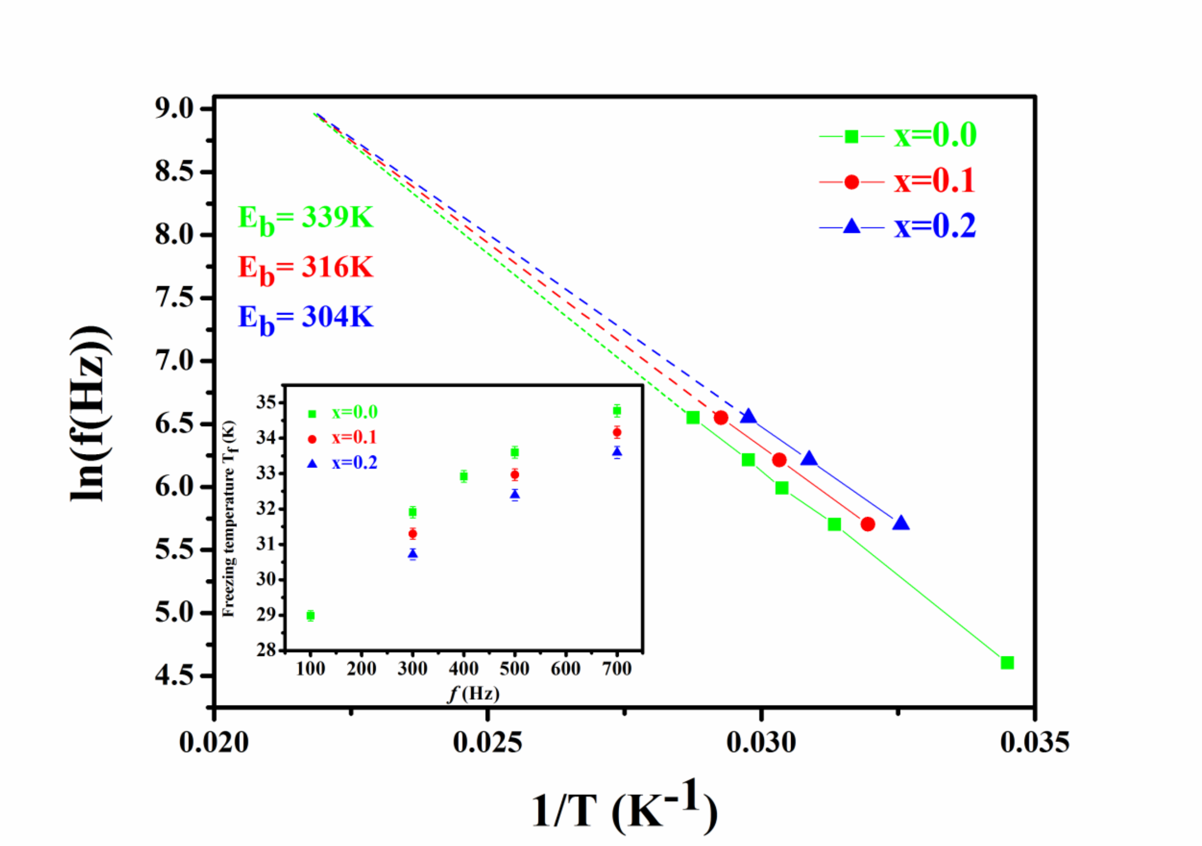

Figure. 4.7: *Arrhenius law fits of frequency dependence of freezing temperatures* T_f *for EFTO (x=0.0, 0.1 and 0.2). Inset: Frequency dependence of* T_f *for pure (x=0.0) and doped samples (x=0.1 and 0.2).*

Further investigations have been done by performing similar ac susceptibility measurements on the sample (ETOF10) with higher Fe concentration i.e. x=0.2 (Fig. 4.8(a-d)). At H=0 Oe, the $\chi^{/}$ and $\chi^{//}$ curves are exhibiting similar behaviour as of ETOF5 sample i.e. appreciable suppression in spin freezing at ~35 K [Fig. 4.8(a-c)] and a further minute shift in T_f (inset of Fig. 4.7). However, the energy E_b as extracted from the Arrhenius fit to the $\chi^{//}$ peaks, has a smaller value E_b=304 K than that of ETOF5 (Fig. 4.7). This eventually suggests a monotonous decreasing trend in CF level spacing with increasing Fe substitution.

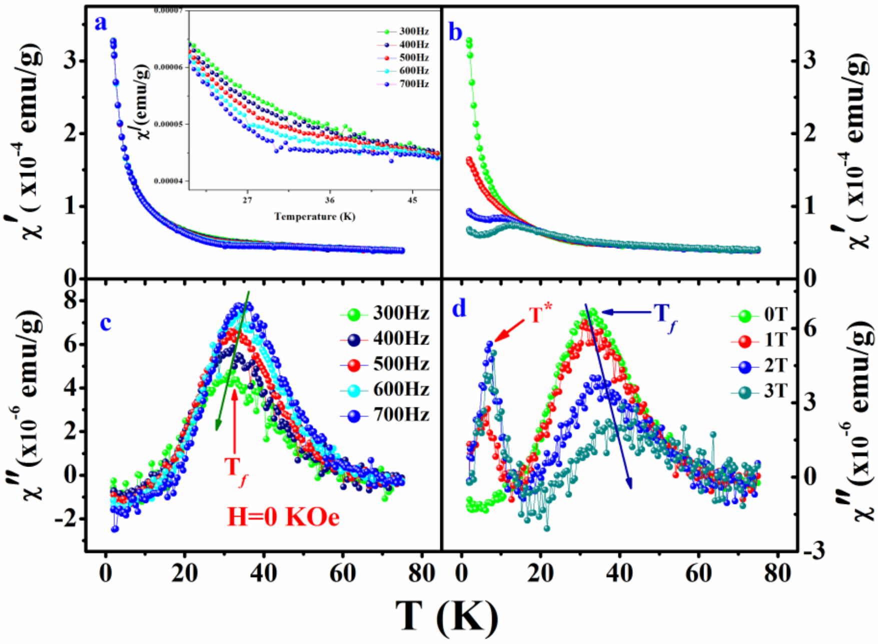

Figure. 4.8 *:(a) and (b) showing the temperature (T) variation of* $\chi^{/}$ *and* $\chi^{//}$ *at dc field H=0 KOe for x=0.2 sample. Fig. (c) and (d) showing* $\chi^{/}$ *(T) and* $\chi^{//}$ *(T) curves with different applied dc fields at frequency 500Hz. Inset of fig (a) : Enlarged view of* $\chi^{/}$ *(T) @H=0 KOe*

Moreover, to get an quantitative idea about how the fundamental nature of the single ion freezing gets affected by Fe doping, we have used Mydosh parameter (p) which is typically used for confirming a spin glass transition: $p = \frac{\Delta\tau_f}{\tau_f \Delta log f}$; where τ_f is the freezing temperature for the frequency f [31]. The analysis yielded a slightly decreased value of the parameter p from ~0.286 (for x=0.0) to ~0.2 for the doped samples. The little decrease in p value can be understood on the basis of the random occupancy of the doped Fe ions which usually contribute towards the typical spin glass state. However, all the p values obtained for our samples are quite large as compared to its value typically found for spin glass compounds i.e. 0.005<p<0.08. Thus, the fundamental nature of the higher temperature spin freezing remained unaffected even after Fe doping.

To investigate how the external magnetic field affects the spin relaxations, we have measured ac susceptibility in presence of magnetic fields. To our surprise, for ETOF5 sample, we have observed an additional clear dip forming a local maxima in $\chi^{/}$ around a temperature T^{*}~4K, for H=1 T while the corresponding peak in $\chi^{//}$ is observed with a narrow and sharp shape [Fig 4.6(b,d)]. Clearly this new peak is associated to a dissipative spin relaxation process which is solely field-induced and purely raised by Fe doping. The absence of frequency dependence in these new peaks rules out the thermally activated process unlike the higher temperature freezing transition (T_f ~35 K). As a matter of fact, the Fe substitution may cause site-randomness of Eu and Fe spins which in turn can raise conventional spin glass freezing. However, the newly observed $\chi^{//}$ peaks do not appear as a glassy transition, firstly as the typical spin glass peaks are quite broad and they are frequency dependent while the observed $\chi^{//}$ peaks are sharp and merely frequency independent (Fig. 4.6d). Secondly, the M(T) curve of ETOF5 has neither showed any anomaly nor any bifurcation between ZFC and FC curves near this temperature T^{*}. Thus, the origin of the observed transition seems to be different than of spin glass. Hence, to further explore the origin, we have investigated the ac susceptibility measurements with increasing dc fields. With increasing fields, $\chi^{/}$ curves are seen to progressively form local maxima below 10 K (Fig. 4.9(a)). On the other hand, the peak position of $\chi^{//}$ shifts towards higher temperature with increasing fields which is in strong contrast to the features of spin glass (Fig. 4.9(c)) [60]. Therefore, all the above features confirm the observed new transition to be solely different from spin glass state. Similarly for ETOF10 sample, on application of dc fields H, similar local maxima in $\chi^{/}$ and the associated peaks in $\chi^{//}$ (6 K<T^{*}<8 K) are observed [Fig. 4.8(b&d)]. The only noticeable difference is that the field induced peaks are observed at relatively higher temperatures for higher doping.

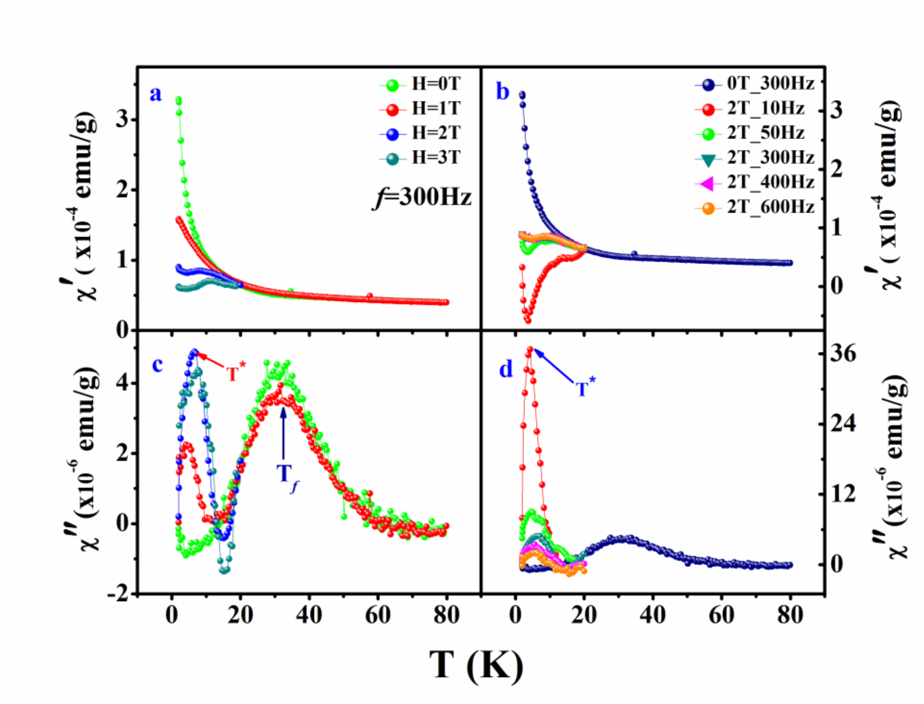

Figure. 4.9: *Field and frequency dependence of* $\chi^{/}$ *and* $\chi^{//}$ *for x=0.1 sample. (a) and (c) showing* $\chi^{/}$ *and* $\chi^{//}$ *as a function of temperature at f=300Hz at different fields. (b) and (d) showing temperature variation of* $\chi^{/}$ *and* $\chi^{//}$ *at dc field H=2T with different frequencies.*

It is pertinent to mention here that in a hybrid pyrochlore system $Dy_xTb_{2-x}Ti_2O_7$ (DTTO), two distinct field induced peaks in ac susceptibility were reported: the single ion freezing peak at 16 K and the field induced peak at ~12 K [61]. The origin of the field induced peak (~12 K) which is associated to Tb^{3+} is still not clear, as it showed unusual jump in the E_b with small amount of Tb^{3+} substitution. However, there are qualitative differences between field induced peaks reported in DTTO and peaks observed in the present EFTO system. Both the observed peaks in DTTO are thermally activated and they are emerged when external field is applied. In contradistinction for the EFTO, only the higher temperature peaks (T_f ~35 K) are thermally activated but the lower temperature (4 K<T^*<8 K)) field induced peaks don’t follow Arrhenius behaviour and thus they are not thermally activated, hence are not related to CF states of Eu^{3+}. Moreover, though the lower temperature (4

K<T^*<8 K) peaks are exclusively originated by external field influence, the higher temperature (T_f~35 K) peaks are not enhanced by external fields unlike in DTTO.

Apart from this, another interesting feature of the new transition is that its $\chi^{//}$ peaks show monotonous growth even down to 10 Hz, in contrast for the higher temperature freezing, $\chi^{//}$ peaks showed progressive suppression with decreasing frequency and finally disappeared below 100 Hz (Fig. 4.9(d)). The $\chi^{/}$ peaks also show relatively larger frequency dispersion as is evident from Fig. 4.9(b). The growing $\chi^{//}$ peaks at such a low frequency (10 Hz) clearly suggests an unusually slow relaxation of spins at this low temperature region (4 K<T^*<8 K). It is in strong contrast with common convention that strong applied magnetic field would cause a faster spin relaxation to achieve an equilibrium spin state. However, the observed phenomena could be explained in different ways. To elucidate the observed slow relaxation, the field induced local maxima in $\chi^{/}$ may be addressed to “single moment saturation” which states “in presence of a sufficiently high field, the susceptibility associated to thermal fluctuations of spins approaches zero both at high temperatures and as T→0 K” [62]. Eventually, such field induced “single moment saturation peaks in $\chi^{/}$” were previously reported in spin liquid $Tb_2Ti_2O_7$ (TTO) and spin ice $Dy_2Ti_2O_7$ at comparatively higher temperatures (T>20 K) [62]. The similar kind of unusually slow spin relaxation was observed in these systems. The origin of such slow relaxation can be explained by the formation of correlated spin-polarized regions inter-linked by strong dipolar interactions, where some spins are polarized along and some are oppositely polarized to the applied field. Hence, due to the presence of large energy barrier to switch these oppositely polarized spins, the relaxation becomes extremely slow and thus the corresponding χ peaks grow even at extremely low frequency. We can reiterate here that rise of dipolar interactions with Fe doping was inferred from earlier dc susceptibility analysis. This can give rise to such spin-polarized regions leading to the observed slow spin relaxation in EFTO. However, the dipolar interaction is still not strong enough as compared to other strongly correlated paramagnets like TTO. However, on looking at the narrow sharp distribution of these $\chi^{//}$ peaks, an alternative explanation which can be evoked is that rise of some type of magnetic ordering. We recall here that rise of magnetic ordering was also predicted from low temperature dc magnetization data which showed sharp rise below 10 K. Also, as already discussed the $\chi^{//}$ peaks were shifted towards higher temperatures with applied dc fields and they were merely frequency independent which are the typical features of magnetic ordering [63]. Hence, development of magnetic ordering can also be a possible origin of the observed transition. Another rare possibility of getting slow spin relaxation may be due to the change in spin-phonon interactions through Fe substitution. Since the mass difference between the two elements is quite large i.e. Eu is almost 3 times heavier than Fe, the Fe substitution would cause appreciable change in the spin phonon spectrum of the system which can result in slow relaxation of the spins. However, more experimental and theoretical investigations may be helpful for further understanding of the underlying physics of the system.

4.4 Conclusion

We have synthesized and characterized the pyrochlore compound of $Eu_{2-x}Fe_xTi_2O_7$ with partial substitution of Fe on Eu site. Electronic structure analysis by XAS study confirmed the elemental nominal oxidation states to be Eu^{3+}, Fe^{3+} and Ti^{4+}. The observation of clear splitting of L_3-e_g peak of Ti 2p XAS spectra has been attributed to the octahedral (O_h) distortion present in TiO_6 octahedra which was also confirmed from XRD data analysis. Additionally, both the Ti$L_{2\text{-}3}$ and O K edge XAS spectra analysis predicted an effective change in the Ti coordination due to migration of oxygen ions to the vacant 8a site leading to anionic disorder and the consequent progressively diminishing O_h distortion with Fe doping. Apart from this, dc magnetization data analysis by a combination of spin-wave and CW models showed that for the doped systems, onset of magnetic ordering starts below 100 K which is mainly due to Eu-Fe interactions. Ac susceptibility study showed large suppression of single ion freezing (T_f ~35 K) owing to the faster spin relaxation of the Fe^{3+} spins, although the fundamental nature of the transition remained unaffected. However, the monotonous decrease in E_b suggests modification crystalline fields of Eu^{3+} spins by Fe doping. Most interestingly, with non zero magnetic fields a new prominent $\chi^{//}$ peak at lower temperatures ($4\ K<T^*<8\ K$) is observed in the doped systems. These new field induced peaks are solely associated to the Fe substitution and not thermally activated unlike single ion freezing at 35 K. The peak positions of these new peaks are shifted to higher temperatures with both increasing doping concentration and applied dc fields. Analysis confirmed it to be completely different from typical spin glass state. Interestingly, the new peaks are associated with an unusually slow spin relaxation. Such slow relaxation is seemingly related to the formation of correlated spin-polarized regions inter-linked by strong dipolar interactions. The new peaks may also refer to a rise of magnetic ordering which was already suggested by dc magnetic data. However, these results indicate the need for detailed study of such systems with combination of different magnetic ions on the single frustrated lattice which has potential to give rise to low temperature exotic states which is absent in similar systems with single magnetic element.

References

1. J. S. Gardner, M. J. P. Gingrasand, J. E. Greedan, Rev. Mod. Phys. **82**, 53(2010).
2. C. Castelnovo, R. Moessner and S L Sondhi, Nature **451**, 42 (2008).
3. S. T. Bramwell, M. J. P. Gingras, Science **294**, 1495 (2001).
4. Y. K. Tsui, C. A. Burns, J. Snyder and P. Schiffer , Phys. Rev. Lett. **82**, 3532(1999).
5. L. Balents, Nature **464**,199 (2010).
6. T. Taniguchi, H. Kadowaki, H. Takatsu, B. Fak, J.Ollivier, T. Yamazaki, T. J. Sato, H.Yoshizawa , Y. Shimura and T.Sakakibara et al, Phys. Rev. B **87**, 060408 (2013).
7. J. S. Gardner, A. Keren, G. Ehlers, C. Stock, E. Segal, J. M. Roper, B. Fak, M. B. Stone, P. R. Hammar, and D. H. Reich et al, Phys. Rev. B **68,** 180401(R) (2003).
8. J. S. Gardner, S. R. Dunsiger, B. D. Gaulin, M. J. P. Gingras, J. E. Greedan, R. F. Kiefl, M. D. Lumsden, W. A. MacFarlane, N. P. Raju, J. E. Sonier, I. Swainson, and Z. Tun, Phys. Rev. Lett. **82**, 1012 (1999).
9. A. P. Ramirez, B. Hessen and M. Winklemann, Phys. Rev. Lett. **84**, 2957 (2000).
10. G. Ehlers, J. E. Greedan, J. R. Stewart, K. C. Rule, P. Fouquet, A. L. Cornelius, C. Adriano, G. Pagliuso, Y. Qiu and J. S. Gardner, Phys. Rev. B **81**, 224405 (2010).
11. B. D. Gaulin, J. N. Reimers, T. E. Mason, J. E. Greedan, and Z. Tun, Phys. Rev. Lett. **69**, 3244 (1992).
12. D. K. Singh, and Y. S. Lee, Phys. Rev. Lett. **109**, 247201 (2012).
13. A. P. Ramirez, G. P. Espinosa, and A. S. Cooper, Phys. Rev. Lett. **64**, 2070 (1990).
14. S. Iguchi, Y. Kumano, K. Ueda, S. Kumakura, and Y. Tokura, Phys. Rev. B **84**, 174416 (2011).
15. P. Schiffer, A. P. Ramirez, D. A. Huse, P. L. Gammel, U. Yaron, D.J. Bishop, and A. J. Valentino, Phys. Rev. Lett. **74,** 2379 (1995).

16. A. P. Ramirez, A. Hayashi, R. J. Cava, R. Siddharthan and B. S. Shastry, Nature **399**, 333 (1999).
17. M. J. Harris, S. T. Bramwell, D. F. McMorrow, T. Zeiske, and K. W. Godfrey, Phys. Rev. Lett. **79**, 2554 (1997).
18. T. A. Bojesen and S. Onoda, Phys. Rev. Lett. **119**,227204(2017).
19. J. Snyder, B. G. Ueland , J. S. Slusky, H. Karunadasa, R. J. Cava, and P. Schiffer, Phys. Rev. B **69**, 064414 (2004).
20. J. Snyder, B. G. Ueland, J. S. Slusky, H. Karunadasa, R. J. Cava, A. Mizel, and P. Schiffer, Phys. Rev. Lett. **91**, 107201 (2003).
21. J. Snyder, J. S. Slusky, R. J. Cava, P. Schiffer,Nature (London) **413**, 48 (2001).
22. J. Oitmaa, R. R. P. Singh, B. Javanparast, A. G. R. Day, B. V. Bagheri, and M. J. P. Gingras, Phys. Rev. B **88,** 220404 (2013).
23. L. Savary, K. A. Ross, B D Gaulin, J P C Ruff and L Balents, Phys Rev Lett, **109,** 167201 (2012).
24. K. E. Sickafus, L. Minervini, R. W. Grimes, J. A. Valdez, M. Ishimaru, F. Li, K. J. McClellan, and T. Hartmann, Science **289,** 748 (2000).
25. J. Lian, J. Chen, L. M. Wang, and R. C. Ewing, Phys. Rev. B **64** 134107(2003).
26. A. Nag (Chattopadhyay), P. Dasgupta, Y. M. Jana, and D. Ghosh, J. All. Comp. **384**, 6 (2004).
27. A. P. Ramirez,Annu. Rev. Mater. Sci. **24,** 453 (1994).
28. G. Ehlers, A. L. Cornelius, T. Fennell, M. Koza, S. T. Bramwell, and J. S. Gardner,J. Phys.: Condens. Matter **16,**S635 (2004).
29. G. Ehlers, A. L. Cornelius , M Orendac, M Kajnakova, T. Fennell, S. T. Bramwell and J. S. Gardner,J. Phys. : Cond. Matt. **15,** L9 (2003).
30. L.D. C. Jaubert, and P. C. Holdsworth,Nat. Phys. **5**, 258 (2009).

31. A. Pal, A. Singh, A. K. Ghosh, S. Chatterjee, J. Magn. Magn. Mater. **462,** 1 (2018).
32. S. Cao, L. Chen, W. Zhao, K. Xu, G. Wang, Y. Yang, B. Kang, H. Zhao, P. Chen, and A. Stroppa, Sci. Rep. **6**, 37529 (2016).
33. H. Wu, S. Cao,M. Liu, Y. Cao, B. Kang, J. Zhang, and W. Ren, Phys. Rev. B **90**, 144415 (2014).
34. T. Aoyama, A. Iyama, K. Shimizu, T. Kimura, Phys. Rev. B **91**, 081107 (2015).
35. J. Hemberger, S. Lobina, H.A. Krug von Nidda, N. Tristan, V.Y. Ivanov,A. A. Mukhin, A.M. Balbashov, A. Loidl, Phys. Rev. B **70** 024414(2004).
36. A.R. Denton, and N. W. Aschroft, Phys. Rev. A **43**, 3161(1991).
37. D. L. Hector, and S. B. Wiggin, J. Solid. State. Chem. **177**, 139 (2004).
38. D. H. Kim, H. J. Lee, G. Kim, Y. S. Koo, J. H. Jung, H. J. Shin, J.-Y. Kim, and J.-S. Kang, Phys. Rev. B **79**, 033402 (2009).
39. V. Kachkanov, M. J. Wallace, G. van der Laan, S. S. Dhesi, S. A. Cavill, Y. Fujiwara and K. P. O’Donnell, Sci. Rep **2**, 969 (2012).
40. G. Drera, L. Sangaletti, F. Bondino, M. Malvestuto, L. Malavasi,Y. Diaz-Fernandez, S. Dash, M. C. Mozzati and P. Galinetto, J. Phys.: Condens. Matter **25**, 075502 (2013).
41. S. Kumar, S. Gautam, G. W. Kim, F. Ahmed, M. S. Anwar , K. H. Chae , H. K. Choi, H. Chung, and B. H. Koo,App. Surf. Sci. **257,** 10557 (2011).
42. A. Chasse, St. Borek, K. M. Schindler, M. Trautmann, M. Huth, F. Steudel, L. Makhova, J. Grafe and R. Denecke, Phys. Rev. B 84 (2011) 195135
43. J. C. Woicik, E. L. Shirley, C. S. Hellberg, K. E. Andersen, S. Sambasivan, D. A. Fischer, B. D. Chapman, E. A. Stern, P. Ryan, D. L. Ederer, and H. Li, Phys. Rev. B **75**, 140103(R) (2007).

44. P. Nachimuthu, S. Thevuthasan, M. H. Engelhard, W. J. Weber, D. K. Shuh, N. M. Hamdan, B. S. Mun, E. M. Adams, D. E. McCready, V. Shutthanandan, et. al. Phys. Rev. B **70** (2004)100101
45. F. M. F. De Groot, M. O. Flgueiredo, M. J. Basto, M. Abbate, H. Petersen and J. C. Fuggle, J. Phys. Chem. Min **19** (1992) 140
46. P. E. R. Blanchard, S. Liu, B. J. Kennedy, C. D. Ling, Z. Zhang, M. Avdeev, B. C. C. Cowie, L. Thomsenc and L. Y. Jangd, Dalton Trans. **42** (2013)14875 and references therein.
47. J. P. Crocombette, and F. Jollet,J. Phys.: Condens. Matter **6**, 10811(1994).
48. P. Krüger, Phys. Rev. B 81, 125121 (2010).
49. M. Umeda, Y. Tezuka, S. Shin, and A. Yagishita, Phys. Rev. B **53**, 1783(1996).
50. K. Okada and A. Kotani,J. Electron Spectrosc. Relat. Phenom. **62,**131(1993).
51. P. E. R. Blanchard; S. Liu; B. J. Kennedy; C. D. Ling; M. Avdeev; J. B. Aitken; B. C. C. Cowie; A. Tadich, J. Phys. Chem. C **117** (2013) 2266.
52. P. Dasgupta, Y. M. Jana, A. N. Chattopadhyay, R. Higashinaka, Y. Maeno and D. Ghosh, J. Phys. Chem. Solid. **68,** 347 (2007).
53. I. O. Troyanchuk, and N. V. Kasper,J. Phys.: Condens. Matter **10**, 401(1998).
54. S. J. Potashnik, K. C. Ku, R. Mahendiran, S. H. Chun, R. F. Wang, N. Samarth, and P. Schiffer, Phys. Rev. B **66**, 012408 (2002).
55. M. J. P. Gingras , B. C. den Hertog, M. Faucher, J. S. Gardner, S. R. Dunsiger, L. J. Chang, B. D. Gaulin, N. P. Raju and J. E. Greedan,Phys. Rev. B **62**, 6496 (2000).
56. N. P. Raju, M. Dion, M. J. P. Gingras, T. E. Mason and J. E. Greedan, Phys. Rev. B **59** 14489 (1999).
57. J.A. Mydosh, J. Magn. Magn. Mater **157/158,** 606(1996).

58. S. T. Bramwell, and M. J. Harris, J. Phys.: Cond. Matt. **10**, L215(1998).
59. J. Snyder, B. G. Ueland, A. Mizel, J. S. Slusky, H. Karunadasa, R. J. Cava and P. Schiffer,Phys. Rev. B **70,** 184431 (2004).
60. K. Manna, A. K. Bera, M. Jain, S. Elizabeth, S. M. Yusuf and P. S. Anil Kumar,Phys. Rev B **91,**224420 (2015).
61. H. Xing, M. He, C. Feng, H. Guo, H. Zeng and Z. Xu, Phys. Rev. B 81, 134426 (2010).
62. B. G. Ueland, G. C. Lau, Phys. Rev. Lett. **96**, 027216(2006).
63. M. L. Dahlberg, M. J. Matthews, P. Jiramongkolchai, R. J. Cava, and P. Schiffer, Phys. Rev. B **83**, 140410(R) (2011).